Enhanced humidity responsive ultrasonically nebulised V_2O_5 thin films

NANO EXPRESS

PAPER

Enhanced humidity responsive ultrasonically nebulised V_2O_5 thin films

Inyalot Jude Tadeo, Rajasekar Parasuraman, Saluru B Krupanidhi and Arun M Umarji

Materials Research Centre, Indian Institute of Science, Bengaluru, 560012, India

E-mail: umarji@iisc.ac.in

Keywords: V_2O_5, nebulized spray pyrolysis, Raman spectroscopy, humidity sensor, sensitivity

OPEN ACCESS

RECEIVED
3 February 2020

REVISED
6 February 2020

ACCEPTED FOR PUBLICATION
18 February 2020

PUBLISHED
16 March 2020

Abstract

A large surface to volume ratio and easily accessible active reaction sites are key attributes for a good gas sensing material. Herein, we report synthesis, characterisation and humidity sensing properties of phase pure 420 nm thick low temperature (350 °C) polycrystalline V_2O_5 thin films deposited on quartz substrate by ultrasonic nebulized spray pyrolysis of aqueous combustion mixture (UNSPACM). The thin films were characterized by x-ray diffraction, Raman spectroscopy, atomic force microscope, field emission scanning microscope, transmission electron microscope, UV–visible spectroscopy and XPS. The highly porous and nanocrystalline characteristic of V_2O_5 thin films synthesized by this technique provide large surface to volume ratio and easily accessible active reaction sites making it a prominent material for gas sensing applications. The fabricated humidity sensor based on V_2O_5 thin films exhibited high sensitivity with good stability and reproducibility at room temperature. The sensor exhibited high sensitivity of 90.8% at 76% RH with response time of 35–60 s and recovery time of 7–54 s. We believe this method provides means for large-scale synthesis of V_2O_5 thin films for several gas sensing applications.

1. Introduction

Several oxides of vanadium such as V_2O_5, VO_2, V_2O_3, and VO exist with unique and interesting properties due to the existence of vanadium in different stable oxidation states (V^{2+} to V^{5+}). Among them, V_2O_5, the most stable oxide, has attracted great interest owing to its layered structural nature, large optical band gap, good thermal stability, chemical stability and excellent electrochromic and thermoelectric characteristics [1–3]. V_2O_5 is known to be an n-type [2, 4, 5] semiconducting material. It crystallizes in *Pmmn* space group of orthorhombic crystal system having lattice parameters of a = 11.510, b = 3.563 and c = 4.369 Å [6]. The 2D layered structure consists of layers weakly bound by the electrostatic forces along *c* axis of unit cell where each unit cell possesses two formula units [2, 6, 7]. Layers build up from VO_5 square pyramidal units sharing edges thereby making double chains along b-direction [6, 8, 9] Chains are linked at the corners forming octahedrally coordinated VO_6 with different vanadium-oxygen distances emanating from three distinct oxygens; terminal V-O_1 (1.58 Å) doubly bound oxygen along c-direction, doubly V-O_2 and triply V-O_3 coordinated (1.77–2.02 Å) bridging oxygen in basal plane and weak V-O (2.79 Å) bonds between the layers [6, 7]. The spacing between the layers provides favorable sites for the intercalation of several species [10] into V_2O_5 making it a favorable material for numerous applications like gas sensing [11, 12], lithium-ion batteries [13] and catalysis [14]. Different synthesis techniques like atomic layer deposition [2], spray pyrolysis [15–20], sol-gel [21], spin coating [22], chemical vapor deposition [3], sputtering [23], pulsed laser deposition [24] and electron beam evaporation [25] are being employed to synthesize V_2O_5 thin films on different substrates. Generally, V_2O_5 thin films deposited at a substrate temperatures <300 °C are amorphous [1]. Crystallization temperature as well as thin film properties like optical band gap have been found to depend on growth method and nature of substrate (amorphous or crystalline) [1, 26]. Highly porous materials [27] most especially metal oxides [28] in thin film form have been

found to exhibit high humidity sensitivity owing to large surface to volume ratio [29, 30] and easy tunability of their optical and electronic properties [31]. Humidity sensors are employed in monitoring and regulating ambient humidity which plays a key role in our daily lives [27, 32]. They are used in numerous fields such as agriculture, semiconductor fabrication, food processing, drug manufacture and storage, preservation of antiques and paintings, cryogenic processes, packaging and regulation of humidity levels in living rooms [27, 33–37]. A semiconducting material possessing large surface to volume ratio coupled with easily accessible redox reaction sites is desirable for gas sensing application [31, 38]. The 2D layered nature and the spacing between layers in V_2O_5 provide favorable sites for the intercalation of several species into it, making V_2O_5 an appealing material for numerous sensing applications.

This work presents synthesis, characterization, and humidity sensing properties of high-quality low temperature (350 °C) polycrystalline V_2O_5 thin films synthesized by UNSPACM, a simple, large area and cost-effective deposition technique. The technique besides being cheap, is scalable, compatible, flexible and yields highly porous films suitable for gas sensing applications due to its enhanced surface to volume ratio. It also provides easy way to dope any element in any stoichiometry of interest through solution [15] without having the need for complex equipment and with no vacuum or special substrate requirements. It further provides an advantage over other reported spray pyrolysis techniques [15, 16, 18–20] by combining solution combustion synthesis (SCS) and spray pyrolysis methods. The self-propagating elevated temperature reaction characteristic of SCS aids complete conversion of precursors into products resulting into high quality thin films [39]. Taking into consideration large area deposition of the films and scalable deposition of V_2O_5 thin films through UNSPACM for industrial applications is less exploited coupled with excellent sensing properties of V_2O_5, it becomes useful to investigate humidity sensing properties of low-cost large area V_2O_5 thin films deposited by this technique. The as-synthesized V_2O_5 thin films were used to fabricate humidity sensor and its sensing properties were studied using an in-house built sensing setup. The V_2O_5 films exhibited enhanced sensitivity, stability, fast response and recovery times towards humidity at ambient conditions without going for tedious complex and complicated lithographic designs and with no special substrate requirement.

2. Experimental

2.1. Synthesis

Porous V_2O_5 thin films were deposited on pre-cleaned quartz substrate at 350 °C by UNSPACM. Precursor solution (aqueous combustion mixture) was made by taking stoichiometric amounts of vanadyl nitrate (oxidizer) and urea (fuel) dissolved in few ml of distilled water. Vanadyl nitrate was obtained by adding few drops of concentrated nitric acid in ammonium metavanadate. Measurements were done ensuring maximum exothermicity whereby the ratio of oxidizer to fuel was one [39]. Reaction scheme leading to the formation of V_2O_5 is as shown below.

$$2VO(NO_3)_3 + 5CH_4N_2O \rightarrow V_2O_5 + 8N_2 + 10H_2O + 5CO_2$$

The precursor solution was taken into specialized glass setup and nebulized using 2.5 MHz frequency ultrasonic nebulizer (Mystique Air Sep USA). The schematic of the setup is given elsewhere [40]. N_2 gas kept at a flow rate of 1000 sccm was used to carry ultrasonically nebulized mist into the substrate kept at 350 °C. The droplets pyrolyzed immediately upon reaching the hot substrate. Film deposition was done for 10 min. V_2O_5 forms when droplets reach the hot substrate owing to the high exothermic and self-propagating nature of the reaction.

2.2. Characterization

Structural analysis of thin films was done using x-ray diffraction X'Pert-PRO PANalytical instrument with Cu-Kα radiation (1.5418 Å) at a scan rate of 2° per minute. Phase formation was further confirmed from Raman spectra of the thin films measured at room temperature in 50–1100 cm^{-1} range (Horiba JobinYvon HR-Raman-123 microPL spectrometer at 532 nm wavelength). Morphology and microstructure of thin films was investigated by Inspect F50 field emission scanning electron microscope and JEOL 2100 F transmission electron microscope operated at 20 and 200 keV respectively. Surface roughness of the films was measured using non-contact mode A.P.E Research A100-AFM atomic force microscope. Veeco Dektak 6 M surface profilometer was used to measure the film thickness. Optical characterization of the thin films was done by Perkin Elmer-Lambda 750 UV-Vis-NIR spectrophotometer. The chemical electronic states of thin films were analyzed by x-ray photoelectron spectroscopy (XPS) measurements conducted using axis ultra DLD (from Kratos) high resolution instrument with automatic charge neutralization equipped with MgKα radiation (1253.5 eV). XPS data was fitted using XPS Peak41 software [41].

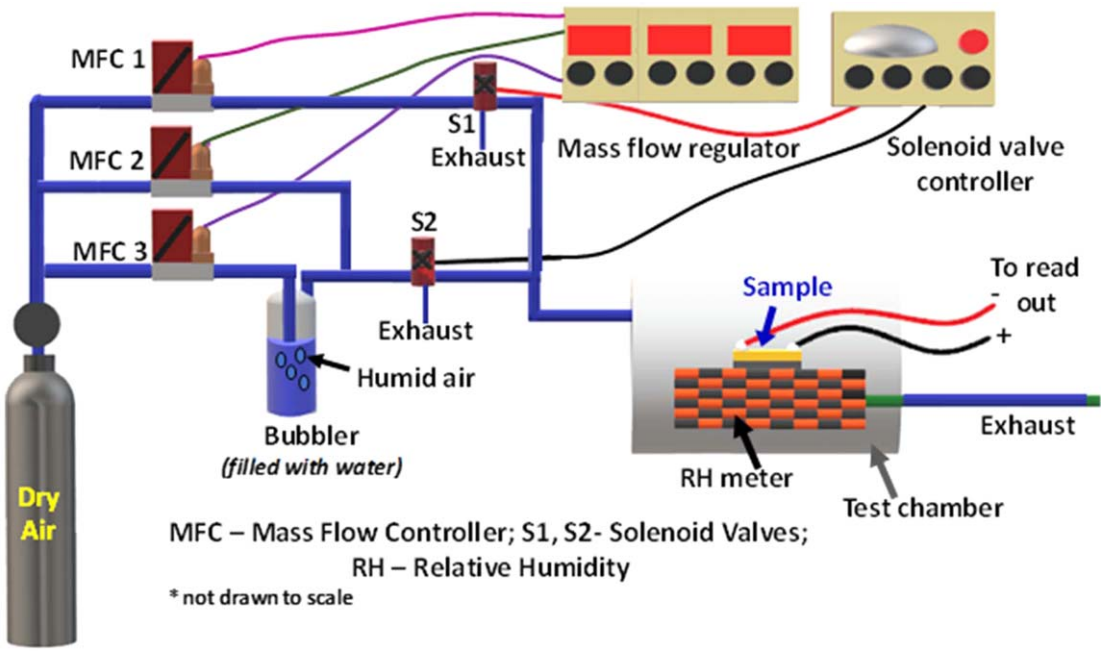

Figure 1. Schematic diagram of an in-house built humidity sensing setup.

2.3. Humidity sensing

Room temperature humidity sensing studies on the films were conducted in a simple in-house built computer-controlled sensing system (figure 1) comprising of dry gas cylinder, mass flow controllers (MFC 1, MFC 2 and MFC 3) attached to mass flow regulator, bubbler containing water, solenoid valves (S1 and S2) attached to solenoid controller, test chamber, sensor holder and data acquisition system. The contacts of the V_2O_5 humidity sensing device were fabricated by applying a small amount of silver paste on corners of V_2O_5 thin film (figure 1). The linear nature of current-voltage curves confirmed the ohmic nature of contacts. The humidity sensing setup has two lines leading to the sample; (i) MFC 1 and S1, and (ii) MFC 2, MFC 3, Bubbler (water) and S2. First line which leads flow of dry air alone is taken as background. Second line is humid air attained by bubbling dry air through MFC 3 in to water, and relative humidity was controlled by adjusting the flow of dry air in MFC 2. The solenoid valves 1 and 2 are coupled through timed solenoid controller, which makes only one line active at a time.

The relative humidity is controlled by dry air flow through MFC 2 and the time of exposure to the humid air is controlled by solenoid valve controller. The RH levels were monitored using Generic E_14009384 220 V Digital Air Humidity Controller. The relative humidity (RH) of 25, 44, 58, 62 and 76% were attained and maintained at room temperature (25 °C). The change in conductivity of V_2O_5 thin film was measured with a Keithley 6430 Source Meter SMU instrument at different RH atmospheres. This setup can be adopted for studying sensing properties of bulk or thin films for volatile organic compounds and other analytes of interest.

3. Results and discussion

3.1. X-ray diffraction

Figure 2(a) shows the XRD pattern of V_2O_5 thin films. The optimized deposition temperature of 350 °C was deduced after depositing thin films at several substrate temperatures (250 °C–450 °C). Films deposited below 350 °C were found to be amorphous while thin films deposited at substrate temperature $\geqslant$ 350 °C were crystalline. Grain growth was seen to increase with deposition temperature. Thin films were polycrystalline and preferentially oriented in (001) direction. This was demonstrated by highest intensity peak at 2θ value of 20.32°. All diffraction peaks were indexed to *Pmmn* space group of orthorhombic V_2O_5 crystal system (JCPDS # 77-2418) [42]. No any characteristic impurity peaks nor of any other vanadium oxides was observed revealing phase purity of synthesized V_2O_5 thin films. Average crystallite size, D of thin films was estimated by Scherrer's formula [43, 44], given by $D = \frac{K\lambda}{(\beta^2-\omega^2)^{1/2}\cos\theta}$ where 2θ is Bragg's angle, K is Scherrer's constant taken in this case to be 0.9 [44], λ represents the wavelength of x-ray radiation used ($CuK_\alpha = 1.5418$ Å), β is the peak's full width at half maximum while ω is instrumental broadening recorded for standard silicon sample. Average D value was determined to be 22 $\pm$ 0.5 nm. Dislocation density, δ expressed as length of dislocation lines per unit

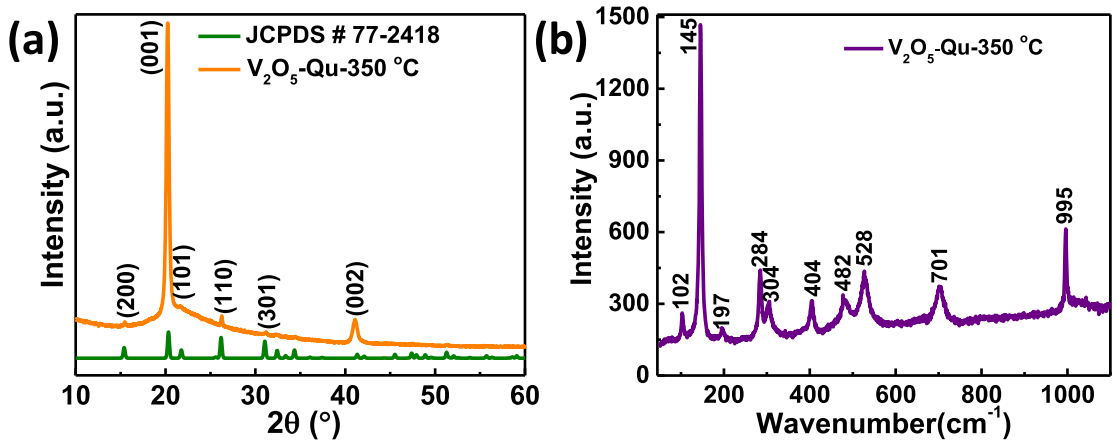

Figure 2. (a) x-ray diffraction pattern and (b) room temperature Raman spectra of V_2O_5 thin films.

Table 1. Raman active modes for as-deposited V_2O_5 thin films.

	Symmetry [6, 46, 47]	Wavenumber (cm^{-1})			
Assignment		Ref [6]	Ref [46]	Ref [47]	**This work**
T_z	A_g	98	101	98	102
T_y, R_z	B_{3g}, B_{2g}	142	145	145	145
T_x, R_y	B_{1g}	194	198	194	197
δ(V=O)b.	B_{2g}, B_{3g}	281	284	281	284
δ(V_3–O)b	A_g	300	305	300	304
δ(V=O)b.	A_g	403	406	405	404
δ(V–O–V)b.	A_g	476	484	470	482
ν(V_3–O)s.	A_g	526	531	520	528
ν(V–O–V)s.	B_{2g}, B_{3g}	698	704	694	701
ν(V=O)s.	A_g	992	996	992	995

A_g mode and 6 modes of B_{1g}, B_{3g} symmetry are not observed.

volume of crystal was calculated from the relation $\delta = \frac{1}{D^2}$ [20, 45] where D is crystallite size and its value was found as $\delta = 2.06 \times 10^{-3}$ lines/nm^2. This small dislocation density confirms good crystallinity of the synthesized V_2O_5 thin films [20]. Achievement of high crystalline films at such a low temperature (350 °C) can be attributed to the exothermic nature of the combustion reaction where the local temperature can be higher.

However, the high temperature exposure lasts for a very short time avoiding crystalline growth, thereby resulting in high surface area. Instantaneous evolution of gases not only results in porous microstructure but also quenches the product thereby preventing grain growth.

3.2. Raman spectroscopy

Phase formation of the thin films was further confirmed from Raman spectroscopic measurements. Figure 2(b) shows Raman spectra of V_2O_5 thin films recorded at room temperature. The Raman spectra of the films featured ten peaks at wavenumbers 102, 145, 197, 284, 304, 404, 482, 528, 701 and 995 cm^{-1} which were consistent with wavenumber values reported for crystalline V_2O_5 [6, 17, 46]. The peaks were assigned to different bending and stretching vibrational modes of V_2O_5 as given in table 1.

3.3. Morphology and microstructure

Figures 3(a) and (b) show the 2D and 3D AFM images of V_2O_5 thin films deposited on quartz substrate at 350 °C. The films had roughness value (rms) of 238 ± 9 nm. The thin films were 420 ± 10 nm thick as determined by Dektak profilometer measurements. The low and high-magnification SEM images of V_2O_5 thin films deposited by UNSPACM technique are presented in figures 3(c) and (d) respectively. They reveal highly porous nature of the thin films, a suitable property for gas sensing applications [3, 27]. The films had average particle size of 296 ± 6 nm measured using image-J software [48]. The TEM image of V_2O_5 nanoparticles is presented in

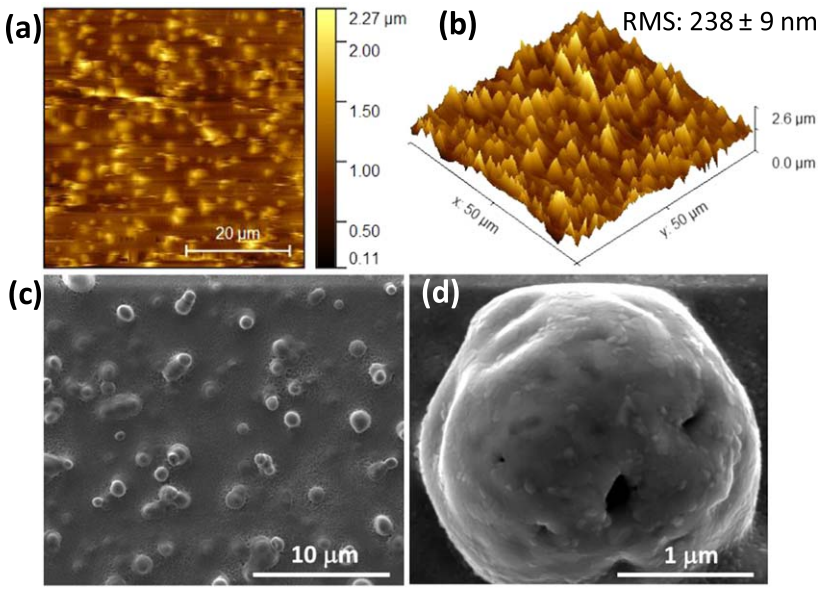

Figure 3. (a) 2D and (b) 3D AFM images, (c) low magnification FESEM image and (d) high magnification FESEM image of V_2O_5 thin films.

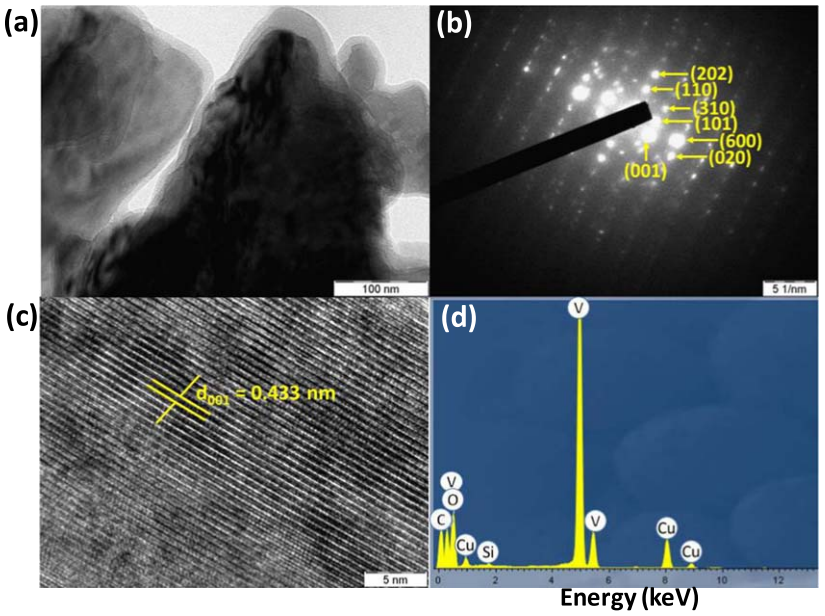

Figure 4. (a) TEM image of synthesized V_2O_5 thin films, (b) Selected area electron diffraction pattern, (c) HRTEM image and (d) EDS spectrum of the sample.

figure 4(a). The selected area electron diffraction (SAED) pattern given in figure 4(b) reveals polycrystalline nature of V_2O_5 thin films. The lattice spacings at 0.433, 0.401, 0.341, 0.261, 0.204, 0.191 and 0.178 nm obtained from selected SAED pattern correspond to d-spacings of (001), (101), (110), (310), (202), (600) and (020) crystal planes respectively proving the polycrystalline characteristic of thin films.

The high-resolution transmission electron microscope image shown in figure 4(c) demonstrates 0.433 nm lattice spacing corresponding to (001) crystal plane indicating preferential orientation of thin films in (001) direction. These observations agree with XRD planes of orthorhombic V_2O_5, space group *Pmmn* shown in figure 2(a). The EDS spectrum is shown in figure 4(d); it confirms the presence of vanadium (V) and oxygen (O) in the sample.

The existence of silicon (Si), carbon (C) and copper (Cu) is due to substrate and carbon-coated copper grids used for TEM analysis.

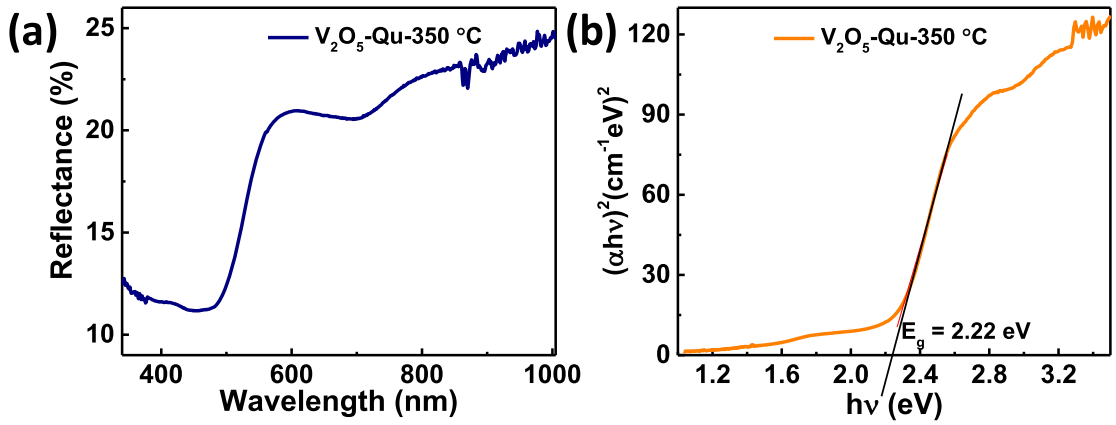

Figure 5. (a) Diffuse reflectance and (b) Tauc plot for synthesized V_2O_5 thin films.

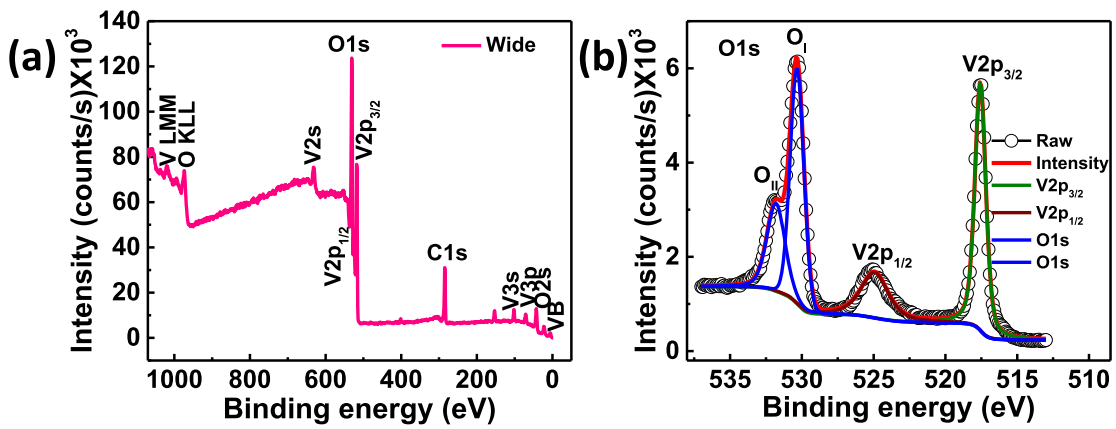

Figure 6. XPS; (a) Survey spectrum and (b) O1s and V2p region for V_2O_5 thin films.

3.4. Optical

Figure 5(a) shows the diffuse reflectance (DRS) of V_2O_5 thin films recorded at 200–1200 nm of wavelength. Kubelka-Munk function, KM was used to convert DRS into absorption spectra [49, 50]. KM at any wavelength is expressed as $F(R_\infty) = \frac{(1-R_\infty)^2}{2R_\infty} = \frac{\alpha}{S}$ where R_∞ is reflectance of the films relative to reference material ($R_{sample}/R_{reference}$), α is absorption coefficient while S is scattering coefficient. The absorption band edge observed at around 560 nm (figure 5(a)) corresponds to the band gap of V_2O_5. The band gap (optical) of V_2O_5 thin films was estimated to be 2.22 eV from the plot of $(\alpha h\nu)^2$ versus $h\nu$ (direct band gap) [51, 52]; then extrapolating linear section of the curve to reach horizontal axis as presented in figure 5(b) (Tauc plot).

This value agrees with reported band gap values for V_2O_5 thin films [1].

3.5. X-ray photoelectron spectroscopy

Figure 6(a) presents survey spectrum of the thin films from which peaks corresponding to O1s, $V2p_{3/2}$ and $V2p_{1/2}$ core-level spectra were identified. The adventitious C1s peak present at binding energy (BE) of 284.8 eV was taken as a reference. O1s and V2p peaks were then calibrated based on this value.

The background was subtracted by applying Shirley background function (figure 6(b)). $V2p_{3/2}$ peak occurred at BE of 517.6 eV with FWHM of 0.9 eV while $V2p_{1/2}$ peak appeared at BE of 524.9 eV with FWHM of 2.3 eV. These peak positions together with the difference in energy between the $V2p_{3/2}$ and $V2p_{1/2}$ peak values which is 7.3 eV are characteristic of V^{5+} oxidation state [2, 53, 54]. The absence of any other oxidation state in the XPS spectra of the sample further confirms the high quality of V_2O_5 thin films. The O1s peak appearing at BE of 530.3 eV with FWHM of 1.1 eV is attributed to lattice oxygen while O1s peak occurring at BE of 531.8 eV with FWHM of 1.5 eV is ascribed to atmospheric oxygen present due to CO_2 or H_2O [55, 56].

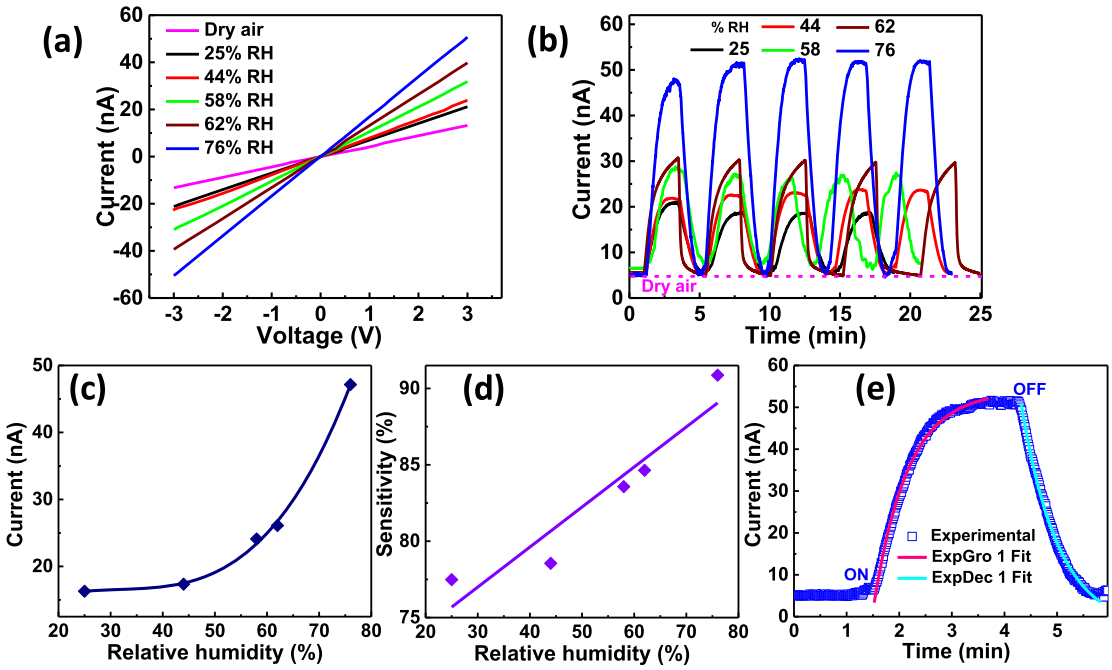

Figure 7. (a) Room temperature current-voltage characteristics of the sensor at different static relative humidity atmospheres, (b) room temperature current-time response curves of the sensor at various RH under 2 V bias voltage, (c) variation of current with relative humidity and (d) sensitivity versus relative humidity, (e) experimental and fitted rise and fall curves for V_2O_5 thin films.

3.6. Sensing

The humidity sensing properties of V_2O_5 thin films were studied by fabricating a two-probe device which was introduced to various relative humidity (RH) environments achieved by mixing dry air with humid air obtained by bubbling dry air through water at a controlled flow rate. The schematic of humidity sensing set up used is given in figure 1. Our method provides an easy way of attaining and maintaining various relative humidity environments thus providing better room for reproducibility of the results. Figure 7(a) shows room temperature current-voltage curves of V_2O_5 based humidity sensor response under different RH environments ranging from dry air to high humid atmosphere (76% RH). The curves are linear proving ohmic characteristic of the contacts. It is also clear from current-voltage curves that current of V_2O_5 humidity sensor increases with increase in relative humidity which is consistent with reports for n-type semiconducting humidity sensors [32].

Further testing was conducted which gave fundamental results on important parameters which characterize sensing device notably sensitivity, response time, recovery time and reproducibility. Figure 7(b) gives device response on exposure to different humidity environments ranging from dry air (5% RH) to various higher RH environments of 25, 44, 58, 62 and 76% at 25 °C. Upon exposure of the device to moist air of 25% RH from dry air (5% RH), current increased drastically and stabilized at a value higher than that exhibited by dry air. Interestingly, on switching off the device back to dry air, current sharply decreased and stabilised at baseline current value of dry air. This quick response and recovery were repeating for several cycles of switching the device from dry air to moist air and vice versa showing greater reproducibility and stability of the sensor; only few representative cycles are given in figure 7(b) to avoid clutter. A similar response trend with enhanced current was noted when the device was subjected to much higher humid air of 44, 58, 62 and 76% RH. The current increased with increase in RH as given in figure 7(c). We tested performance of the device after four months and results were repeating, which further confirms its greater stability and reproducibility.

Conductivity of semiconductor device sensors is dependent upon the humidity levels the sensor is subjected to; it can be electronic or protonic [27, 32]. Water adsorption in V_2O_5 is considered as an intercalation phenomenon to form $V_2O_5.nH_2O$ due to its layered structural nature [1, 3]. On exposure to low humidity atmospheres, less quantity of water molecules get trapped into the layers. They are too far apart for H^+ to move freely between immobile chemisorbed and first physisorbed water layers. Electron hoping thus prevails characterised by low sensor conductivity [32]. At high humidity levels large quantity of water molecules gets intercalated, protons freely move at higher-level physisorbed water layers according to Grotthuss mechanism [32, 57] and protonic conductivity prevails over electronic one. The formation of more physisorbed water layers at higher humidity enhances diffusion of protons through array of hydrogen-bonded water molecules which leads to increased protonic conductivity [58]. The high conductivity at higher humid environments is due electrons donated by the more physisorbed water molecules onto n-type V_2O_5 thereby pushing Femi level closer

Table 2. Comparison of the performance of our device with different oxide-based humidity sensors.

Sensing material	Response time (s)	Recovery time (s)	Sensitivity (at% RH)
SnO_2 nanowires [62]	20–170	20–60	32 (at 85)
ZnO thick films [59]	89	175	0.61 (at 80)
SnO_2/PANI composite [60]	26	30	10 (at 95)
MoO_3 nanorods [61]	118	5	229 (at 97.3)
ZnO nanofeathers [65]	40–70	80–150	229 (at 97)
VO_2(M) nanostructures [64]	5–8	2–3	50 (at 97)
V_2O_5 thin films [2]	2–3	0.5–1	12 (at 95)
V_2O_5 nanotubes [3]	8–12	20–25	90 (at 97.2)
V_2O_5 nanosheets [29]	240	300	43 (at 97.3)
V_2O_5 thin films (**present work**)	35–60	7–54	90.8 (at 76)

to the conduction band thereby enhancing conductivity of the sensor with increasing RH [2]. The sensitivity of the device was determined from the relation $S(\%) = \frac{100(R_H - R_A)}{R_A}$ [29,59–61] where R_H is resistance of sensor at different RH and R_A is resistance of sensor in dry air. Sensitivity was found to be linearly dependent on RH as given in figure 7(d). The V_2O_5 humidity sensor exhibited maximum sensitivity of 90.8% at 76% RH, which is better than that previously reported [2, 29]. Response time and recovery time (defined as time required to reach 90% of final equilibrium value) [62] were determined by fitting one cycle of RH response curves (figure 7(e)) for rise and fall rate constants using first order differential equations expressed as $I(t)_{rise} = I_{dry\ air} + \alpha e^{(t/\tau)}$ and $I(t)_{fall} = I_{dry\ air} + \beta e^{(-t/\tau)}$ respectively [63] where α and β are scaling constants, τ is time constant, t is time for ON or OFF cycles and $I_{dry\ air}$ is sensor current in dry air. The response time and recovery time were determined to be 35–60 s and 7–54 s respectively. We have compared the performance of our device with that of previously reported oxide-based humidity sensors in table 2 [2, 3, 29, 59–62, 64, 65]. Our device exhibits high sensitivity (90.8%) at relatively low RH (76%) which signifies better humidity sensing performance than that of V_2O_5 thin films/nanosheets [2, 29] and other previously reported oxide based humidity sensors [59, 60, 62, 64]. The response/recovery times of our device are also faster than those of other oxide-based humidity sensors reported [29, 59, 61, 62, 65].

This deposition technique provides a simple and cost-effective scalable way of synthesizing V_2O_5 thin films for various sensing applications. The films obtained were highly porous and nanocrystalline in nature, which provides large surface to volume ratio and easily accessible active sites making this a prominent deposition technique for various gas sensing applications. Gas sensing set up described in this work can easily be adopted for sensing various volatile organic compounds, by simply keeping analyte of interest in the bubbler.

4. Conclusion

We have synthesized and comprehensively characterized low temperature (350 °C) crystalline V_2O_5 thin films on quartz substrate by simple and cost-effective deposition technique; ultrasonic nebulized spray pyrolysis of aqueous combustion mixture. The thin films were characterized by XRD, Raman spectroscopy, UV-Visible spectroscopy, scanning electron microscope and transmission electron microscope. Morphological investigation revealed porous and nanocrystalline nature of V_2O_5 thin films, a suitable phenomenon for gas sensing performance due to their enhanced surface to volume ratio. In-house built setup was used to study humidity sensing properties of thin films. The fabricated humidity sensor based on the as-synthesized V_2O_5 thin films demonstrated excellent humidity sensing properties. It exhibited fast response and recovery time of 35–60 s and 7–54 s respectively and high sensitivity of 90.8% at 76% RH. These results exhibit high performance of V_2O_5 thin films opening avenues for large-scale preparation of V_2O_5 thin films for several sensing applications.

Acknowledgments

The authors acknowledge Division of Chemical Sciences and Micro and Nano Characterisation Facility (MNCF) at Centre for Nano Science and Engineering (CeNSE), Indian Institute of Science, Bengaluru for providing TEM

and XPS facilities respectively. Funding from FIST for XRD, SEM and UV-Visible facilities is highly appreciated. Inyalot Jude Tadeo thanks Indian Institute of Science, Bengaluru through the office of international relations for providing him PhD scholarship. Rajasekar Parasuraman acknowledges University Grants Commission (UGC), India for PhD fellowship. Saluru B Krupanidhi greatly acknowledges Fellowship Grant received from Indian National Science Academy.

ORCID iDs

Inyalot Jude Tadeo https://orcid.org/0000-0001-6680-0308
Saluru B Krupanidhi https://orcid.org/0000-0001-6393-0908
Arun M Umarji https://orcid.org/0000-0002-3167-7060

References

[1] Beke S 2011 A review of the growth of V_2O_5 films from 1885 to 2010 *Thin Solid Films* **519** 1761–71
[2] Sreedhara M B, Ghatak J, Bharath B and Rao C N R 2017 Atomic layer deposition of ultrathin crystalline epitaxial films of V_2O_5 *ACS Appl. Mater. Interfaces* **9** 3178–85
[3] Yin H, Yu K, Peng H, Zhang Z, Huang R, Travas-Sejdic J and Zhu Z 2012 Porous V_2O_5 micro/nano-tubes: synthesis via a CVD route, single-tube-based humidity sensor and improved Li-ion storage properties *J. Mater. Chem.* **22** 5013
[4] Faia P M, Libardi J and Louro C S 2016 Effect of V_2O_5 doping on p- to n-conduction type transition of TiO_2:WO_3 composite humidity sensors *Sensors Actuators, B Chem.* **222** 952–64
[5] Meyer J, Zilberberg K, Riedl T and Kahn A 2011 Electronic structure of Vanadium pentoxide: an efficient hole injector for organic electronic materials *J. Appl. Phys.* **110** 033710
[6] Baddour-Hadjean R, Golabkan V, Pereira-Ramos J P, Mantoux A and Lincot D 2002 A Raman study of the lithium insertion process in vanadium pentoxide thin films deposited by atomic layer deposition *J. Raman Spectrosc.* **33** 631–8
[7] Haber J, Witko M and Tokarz R 1997 Vanadium pentoxide I. Structures and properties *Appl. Catal. A Gen.* **157** 3–22
[8] Surnev S, Ramsey M G and Netzer F P 2003 Vanadium oxide surface studies *Prog. Surf. Sci.* **73** 117–65
[9] Lee S H, Cheong H M, Seong M J, Liu P, Tracy C E, Mascarenhas A, Pitts J R and Deb S K 2003 Raman spectroscopic studies of amorphous vanadium oxide thin films *Solid State Ionics* **165** 111–6
[10] Livage J 1991 Vanadium Pentoxide Gels *Chem. Mater.* **3** 578–93
[11] Mane A A, Suryawanshi M P, Kim J H and Moholkar A V 2017 Fast response of sprayed vanadium pentoxide (V_2O_5) nanorods towards nitrogen dioxide (NO_2) gas detection *Appl. Surf. Sci.* **403** 540–50
[12] Vijayakumar Y, Mani G K, Reddy M V R and Rayappan J B B 2015 Nanostructured flower like V_2O_5 thin films and its room temperature sensing characteristics *Ceram. Int.* **41** 2221–7
[13] Wang Y, Takahashi K, Shang H and Cao G 2005 Synthesis and electrochemical properties of vanadium pentoxide nanotube arrays *J. Phys. Chem. B* **109** 3085–8
[14] Khodakov A, Olthof B, Bell A T and Iglesia E 1999 Structure and catalytic properties of supported vanadium oxides: support effects on oxidative dehydrogenation reactions *J. Catal.* **181** 205–16
[15] Zhu Y, Choi S H, Fan X, Shin J, Ma Z, Zachariah M R, Choi J W and Wang C 2017 Recent progress on spray pyrolysis for high performance electrode materials in lithium and sodium rechargeable batteries *Adv. Energy Mater.* **7** 1–41
[16] Irani R, Rozati S M and Beke S 2013 Structural and optical properties of nanostructural V_2O_5 thin films deposited by spray pyrolysis technique: Effect of the substrate temperature *Mater. Chem. Phys.* **139** 489–93
[17] Tadeo I J, Mukhokosi E P, Krupanidhi S B and Umarji A M 2019 Low-cost VO_2(M1) thin films synthesized by ultrasonic nebulized spray pyrolysis of an aqueous combustion mixture for IR photodetection *RSC Adv.* **9** 9983–92
[18] Abd–Alghafour N M, Ahmed N M, Hassan Z and Mohammad S M 2016 Influence of solution deposition rate on properties of V_2O_5 thin films deposited by spray pyrolysis technique *AIP Conf. Proc.* **1756** 090010
[19] Benkahoul M, Zayed M K, Solieman A and Alamri S N 2017 Spray deposition of V_4O_9 and V_2O_5 thin films and post-annealing formation of thermochromic VO_2 *J. Alloys Compd.* **704** 760–8
[20] Vijayakumar Y, Reddy K N and Moholkar A V 2015 Influence of the substrate temperature on the structural, optical and thermoelectric properties of sprayed V_2O_5 thin films *Mater. Technol.* **49** 371–6
[21] Beke S, Korösi L, Papp S, Oszkó A and Nánai L 2009 XRD and XPS analysis of laser treated vanadium oxide thin films *Appl. Surf. Sci.* **255** 9779–82
[22] Passerini S, Chang D, Chu X, Le B and Smyrl W 1995 Spin-coated V_2O_5 xerogel thin films. 1. microstructure and morphology *Chem. Mater.* **7** 780–5
[23] Navone C, Baddour-Hadjean R, Pereira-Ramos J P and Salot R 2005 High-performance oriented V_2O_5 thin films prepared by DC sputtering for rechargeable lithium microbatteries *J. Electrochem. Soc.* **152** A1790–6
[24] Ramana C V, Smith R J, Hussain O M, Massot M and Julien C M 2005 Surface analysis of pulsed laser-deposited V_2O_5 thin films and their lithium intercalated products studied by Raman spectroscopy *Surf. Interface Anal.* **37** 406–11
[25] Kumar A, Singh P, Kulkarni N and Kaur D 2008 Structural and optical studies of nanocrystalline V_2O_5 thin films *Thin Solid Films* **516** 912–8
[26] Bahlawane N and Lenoble D 2014 Vanadium Oxide Compounds: Structure, Properties, and Growth from the Gas Phase *Chem. Vap. Depos.* **20** 299–311
[27] Farahani H, Wagiran R and Hamidon M N 2014 Humidity sensors principle, mechanism, and fabrication technologies: a comprehensive review *Sensors (Switzerland)* **14** 7881–939
[28] Li F, Yao X, Wang Z, Xing W, Jin W, Huang J and Wang Y 2012 Highly porous metal oxide networks of interconnected nanotubes by atomic layer deposition *Nano Lett.* **12** 5033–8
[29] Pawar M S, Bankar P K, More M A and Late D J 2015 Ultra-thin V_2O_5 nanosheet based humidity sensor, photodetector and its enhanced field emission properties *RSC Adv.* **5** 88796–804

[30] Jalal A H, Alam F, Roychoudhury S, Umasankar Y, Pala N and Bhansali S 2018 Prospects and challenges of volatile organic compound sensors in human healthcare *ACS Sens.* **3** 1246–63
[31] Erande M B, Pawar M S and Late D J 2016 Humidity sensing and photodetection behavior of electrochemically exfoliated atomically thin-layered black phosphorus nanosheets *ACS Appl. Mater. Interfaces* **8** 11548–56
[32] Chen Z and Lu C 2005 Humidity sensors: a review of materials and mechanisms *Sens. Lett.* **3** 274–95
[33] Yamazoe N and Shimizu Y 1986 Humidity sensors: principles and applications *Sens. Actuators* **10** 379–98
[34] Mukode S and Futata H 1989 Semiconductive humidity sensor *Sens. Actuators* **16** 1–11
[35] Wang Z, Fan X, Li C, Men G, Han D and Gu F 2018 Humidity-sensing performance of 3DOM WO_3 with controllable structural modification *ACS Appl. Mater. Interfaces* **10** 3776–83
[36] Li G Y, Ma J, Peng G, Chen W, Chu Z Y, Li Y H, Hu T J and Li X D 2014 Room-temperature humidity-sensing performance of SiC nanopaper *ACS Appl. Mater. Interfaces* **6** 22673–9
[37] Fu X Q, Wang C, Yu H C, Wang Y G and Wang T H 2007 Fast humidity sensors based on CeO_2 nanowires *Nanotechnology* **18** 145503
[38] Miao J, Cai L, Zhang S, Nah J, Yeom J and Wang C 2017 Air-stable humidity sensor using few-layer black phosphorus *ACS Appl. Mater. Interfaces* **9** 10019–26
[39] Patil K C, Hegde M S, Rattan T and Aruna S T 2008 *Chemistry of Nanocrystalline Oxide Materials - Combustion Synthesis, Properties and Applications* (Singapore: World Scientific Publishing Co. Pte. Ltd)
[40] Kamble V B and Umarji A M 2013 Gas sensing response analysis of p-type porous chromium oxide thin films *J. Mater. Chem. C* **1** 8167
[41] Bharathi R, Naorem R and Umarji A M 2015 Metal-insulator transition characteristics of vanadium dioxide thin films synthesized by ultrasonic nebulized spray pyrolysis of an aqueous combustion mixture *J. Phys. D: Appl. Phys.* **48** 305103
[42] Pan K-Y and Wei D-H 2016 Optoelectronic and electrochemical properties of vanadium pentoxide nanowires synthesized by vapor-solid process *Nanomaterials* **6** 140
[43] Langford J I and Wilson A J C 1978 Scherrer after sixty years: a survey and some new results in the determination of crystallite size *J. Appl. Crystallogr.* **11** 102–13
[44] Monshi A, Foroughi M R and Monshi M R 2012 Modified Scherrer equation to estimate more accurately nano-crystallite size using XRD *World J. Nano Sci. Eng.* **2** 154
[45] Margoni M M, Mathuri S, Ramamurthi K, Babu R R and Sethuraman K 2016 Investigation on the pure and fluorine doped vanadium oxide thin films deposited by spray pyrolysis method *Thin Solid Films* **606** 51–6
[46] Su Q, Huang C K, Wang Y, Fan Y C, Lu B A, Lan W, Wang Y Y and Liu X Q 2009 Formation of vanadium oxides with various morphologies by chemical vapor deposition *J. Alloys Compd.* **475** 518–23
[47] Castriota M, Cazzanelli E, Fasanella A and Teeters D 2014 Electrical conductivity and Raman characterization of V_2O_5 grown by sol-gel technique inside nanoscale pores *Thin Solid Films* **553** 127–31
[48] Schneider C A, Rasband W S and Eliceiri K W 2012 NIH Image to ImageJ: 25 years of image analysis *Nat. Methods* **9** 671–5
[49] Fuller M P and Griffiths P R 1978 Diffuse Reflectance Measurements by Infrared Fourier Transform Spectrometry *Anal. Chem.* **50** 1906–10
[50] Džimbeg-malčić V, Barbarić-mikočević Ž and Itrić K 2011 Kubelka-Munk theory in describing optical properties of paper (1) *Tech. Gaz.* **18** 117–24
[51] Viezbicke B D, Patel S, Davis B E and Birnie D P 2015 Evaluation of the Tauc method for optical absorption edge determination: ZnO thin films as a model system *Phys. Status Solidi* **11** 1700–10
[52] Chand P, Gaur A and Kumar A 2013 Structural, optical and ferroelectric behavior of hydrothermally grown ZnO nanostructures *Superlattices Microstruct.* **64** 331–42
[53] Silversmit G, Depla D, Poelman H, Marin G B and De Gryse R 2004 Determination of the V2p XPS binding energies for different vanadium oxidation states (V^{5+} to V^{0+}) *J. Electron Spectros. Relat. Phenomena* **135** 167–75
[54] Hryha E, Rutqvist E and Nyborg L 2012 Stoichiometric vanadium oxides studied by XPS *Surf. Interface Anal.* **44** 1022–5
[55] Ureña-Begara F, Crunteanu A and Raskin J P 2017 Raman and XPS characterization of vanadium oxide thin films with temperature *Appl. Surf. Sci.* **403** 717–27
[56] Raghu A V, Karuppanan K K and Pullithadathil B 2018 Highly sensitive, temperature-independent Oxygen gas sensor based on anatase TiO_2 nanoparticle grafted, 2D mixed valent VO_x nanoflakelets *ACS Sens.* **3** 1811–21
[57] Miyake T and Rolandi M 2016 Grotthuss mechanisms: from proton transport in proton wires to bioprotonic devices *J. Phys. Condens. Matter* **28** 023001
[58] Liang J G, Wang C, Yao Z, Liu M Q, Kim H K, Oh J M and Kim N Y 2018 Preparation of ultrasensitive humidity-sensing films by aerosol deposition *ACS Appl. Mater. Interfaces* **10** 851–63
[59] Yawale S P, Yawale S S and Lamdhade G T 2007 Tin oxide and zinc oxide based doped humidity sensors *Sensors Actuators, A Phys.* **135** 388–93
[60] Shukla S K, Shukla S K, Govender P P and Agorku E S 2016 A resistive type humidity sensor based on crystalline tin oxide nanoparticles encapsulated in polyaniline matrix *Microchim. Acta* **183** 573–80
[61] Khandare L, Terdale S S and Late D J 2016 Ultra-fast α-MoO_3 nanorod-based humidity sensor *Adv. Device Mater.* **2** 15–22
[62] Kuang Q, Lao C, Wang Z L, Xie Z and Zheng L 2007 High-sensitivity humidity sensor based on a single SnO_2 nanowire *J. Am. Chem. Soc.* **129** 6070–1
[63] Murali B and Krupanidhi S B 2013 Facile synthesis of Cu_2CoSnS_4 nanoparticles exhibiting red-edge-effect: Application in hybrid photonic devices *J. Appl. Phys.* **114** 144312
[64] Yin H, Yu K, Zhang Z, Zeng M, Lou L and Zhu Z 2011 Humidity sensing properties of flower-like VO_2(B) and VO_2(M) nanostructures *Electroanalysis* **23** 1752–8
[65] Zhang N, Yu K, Zhu Z and Jiang D 2008 Synthesis and humidity sensing properties of feather-like ZnO nanostructures with macroscale in shape *Sensors Actuators A* **143** 245–50